Aggregation-induced emission of luminol: a novel strategy for fluorescent ratiometric detection of ALP and As(V) with high sensitivity and selectivity

Yuan-Jun Tong,[a] Lu-Dan Yu,[a] Lu-Lu Wu,[a] Shu-Ping Cao,[a] Ru-Ping Liang,[a] Li Zhang,[a] Xing-Hua Xia,[b]* Jian-Ding Qiu[a]*

[a] College of Chemistry, Nanchang University, Nanchang 330031, China

[b] State Key Laboratory of Analytical Chemistry for Life Science, School of Chemistry and Chemical Engineering, Nanjing University, Nanjing 210093, China

*Corresponding authors. Tel/Fax: +86-791-83969518. E-mail: jdqiu@ncu.edu.cn; xhxia@nju.edu.cn.

Materials and Reagents. Guanine monophosphate (GMP), luminol, thrombin, bovine serum albumin (BSA), immunoglobulin G (IgG), concanavalin A (Con A), horseradish peroxidase (HRP), acetylcholinesterase (AchE), hemoglobin (Hb), glucoamylase (GA), celluase, lipase (LP), sodium orthovanadate (Na_3VO_4), dimethoate, and $Tb(NO_3)_3 \cdot 6H_2O$ were purchased from Sigma-Aldrich. The alkaline phosphatase kit was purchased from Nanjing Jiancheng Institute of Biological Engineering. Other chemicals were analytical grade and used without further purification. All suspensions were prepared using ultrapure water (18.2 MΩ cm) from a Millipore Milli-Q system.

Apparatus. The UV-vis spectra were collected on an UV-2450 spectrophotometer (Shimadzu, Japan). Quanta 200 scanning electron microscopy (SEM, U.S.A.), JEOL2010 transmission electron microscope (TEM, Japan) were used to characterize the size and morphology of the lanthanide coordination polymer nanoparticles. Fourier transform infrared (FT-IR) spectra were obtained using a Nicolet 5700 FT-IR spectrometer. Fluorescence spectra were performed on an F-7000 fluorescence spectrometer (Hitachi, Japan). The excitation wavelength, slit widths (including excitation and emission), and the photomultiplier tube (PMT) voltage were set at 290 nm, 5 nm and 400 V, respectively. To assess accuracy of the method, real samples were also analyzed on an inductively coupled plasma mass spectrometry (ICP-MS) (iCAP Q, Thermo Fisher, America). The luminescence decay measurements were carried out by time-correlated single photon counting (TCSPC) using a horiba jobin yvon fluoromax 3 with a FluoroHub module. Z-average size data were acquired using an

ELS-8000 instrument (Otsuka Electronics, Japan).

Preparation of Luminol-Tb-GMP CPNPs. The luminol-Tb-GMP CPNPs were synthesized through self-assembly of luminol and GMP ligands with Tb^{3+} ions. Initially, luminol (10 mM, 40 μL) was added into GMP (100 mM, 100 μL), and the resulting mixture was incubated for 30 min. An aqueous solution of $Tb(NO_3)_3 \cdot 6\ H_2O$ (100 mM, 100 μL) was then added into the mixed solution of GMP and luminol, forming a white flocculent suspension under stirring at room temperature. The formed white flocculent suspension was diluted by Tris buffer solution (10 mM, pH 9.0) to 1 mL. Finally, the as-synthesized luminol-Tb-GMP CPNPs were stored at 4 °C. The procedure of preparing GMP-Tb CPNPs was similar to luminol-Tb-GMP CPNPs but without addition of luminol.

Ratiometric ALP Activity Assay. The luminol-Tb-GMP CPNPs stock suspension (10 μL) and ALP with different concentrations were orderly added into 40 μL of Tris-HCl buffer (10 mM, pH 9.0), and the mixture was diluted with ultrapure water to controlled a volume of 200 μL. After the suspension was incubated for 20 min, fluorescence spectra was measured with excitation at 290 nm. Then, the ratiometric ALP activity assay in buffer suspension was performed, the fluorescence intensity of the mixtures was measured, showing increase at 432 nm and at 490, 549, 588, and decrease at 632 nm with different concentrations of ALP.

Real Sampling and Sample Prepared for ALP. For the dynamic monitoring ALP in real samples, Runxi Lake (a lake near Nanchang University), the surface waters were collected at 8:00 in the morning from March 3 to April 1, 2018. To avoid the probability

for the inactivation of ALP during storage, we filled the brown bottles completely to minimize headspace and to exclude ambient air. Immediately after collection, they were filtered through the 0.22 μM filters to remove bacteria and precipitate-insoluble large fragments. Because the initial concentration of ALP was too high to detecting of our method, the filtrates were diluted 100 folds with ultrapure water . In addition, in order to avoid long storage time that changed the enzyme activity, the diluted solution of lake water was then taken for experimentation as soon as possible.

As(V) Investigation. To study the application of our established fluorescent approach for As(V) detection, 50 μL aqueous As(V) solutions with different concentrations varying from 0 ppb to 200 ppb were added into 50 μL ALP solution (100 U/L). Next, the mixed solution of ALP with As(V) was incubated at 37 °C for 20 min. Finally, 10 μL luminol-Tb-GMP CPNPs was added into the mixture solution of ALP with As(V), and the mixtures were diluted with Tris buffer to reach 200 μL. The resulting mixtures were allowed to stand by for 20 min and then were used for fluorescent measurements.

Analysis of Water Samples. Tap water, Ganjiang River water and Poyang Lake water were used as real samples. The water samples were first filtered by a 0.22 μm membrane to detach the suspension and solid impurities. Briefly, water samples (100 μL) with standard As(V) solutions from 0 ppb to 20 ppb with ALP were incubated at 37 °C for 20 min. Next, 10 μL luminol-Tb-GMP CPNPs was added into the standard solution, and the mixtures were diluted with Tris buffer to reach 200 μL, and the concentration of ALP was controlled at 50 U/L finally. Then, the fluorescence intensity

of the mixtures were used for fluorescence measurements. To assess accuracy of the method, real samples were also analyzed by ICP-MS.

Scheme S1. (A) The AIE mechanism of luminol with Tb^{3+}. (B) Sensing process for ALP detection based on the AIE mechanism of luminol with Tb^{3+}.

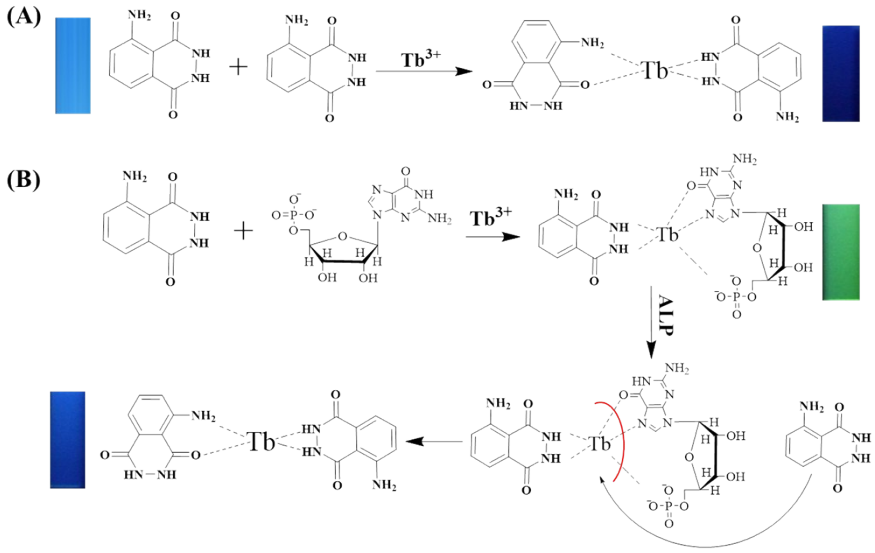

Characterization. GMP-Tb CPNPs were further analyzed by SEM (Figure S1A), which shows a tight net structure with diameters ranging from 40 to 50 nm of colloidal spheres. In order to further certify the formation of luminol-Tb-GMP CPNPs, FT-IR spectra of GMP, luminol and luminol-Tb-GMP CPNPs are displayed in Figure S1B. The peaks at 3420, 3330, 1622, 1053 cm^{-1} of luminol (curve a) are assigned to the N-H stretching modes, N-H stretching modes, C=O stretching vibrations and NH_2 rocking vibrations, respectively.[1] For GMP, the peaks at 1688, 1475, 1240, and 1083 cm^{-1} (curve b) are assigned to the P−OH stretching band (νP−OH), N_7−C_8 stretching (νN_7−C_8) band in the guanine subunit, the phosphate antisymmetric ($vasPO_2$), and symmetric ($vsPO_2$), respectively.[2] For luminol-Tb-GMP CPNPs, the corresponding peaks at 1688, 1475, 1240, and 1083 cm^{-1} (curve c) of GMP are slightly shifted,

suggesting that the phosphate groups and nucleobase moieties of GMP are involved in the coordination process.[3] Meanwhile, the typical peaks of the amino group in the luminol standard FT-IR spectrum at 3420, 3330 and 1053 cm^{-1} are all disappeared or shifted, respectively, which is a reflection of the covalent interaction between the amino group and the Tb^{3+} ions.[4] In addition, in the spectrum of luminol-Tb-GMP CPNPs, the peak at around 1622 cm^{-1} of the stretching vibrations of C=O is slightly shifted, which provides evidence of the successful preparation of luminol-Tb-GMP CPNPs.[2a]

The formation of luminol-Tb-GMP CPNPs was further confirmed by UV–vis spectra (Figure S1C). GMP exhibits a strong absorption peak at 260 nm (curve a), which is ascribed to the π–π* transition of adenine bases.[5] The absorption peak at 300 nm and 347 nm are the characteristic peaks of luminol (curve b).[6] The luminol-Tb-GMP CPNPs (curve d) shows a broaden UV absorption peak and an obvious hypochromic effect at 260 nm and 347 nm (curve d), suggesting the coordinative complexation between GMP and luminol with Tb^{3+} ions.[3]

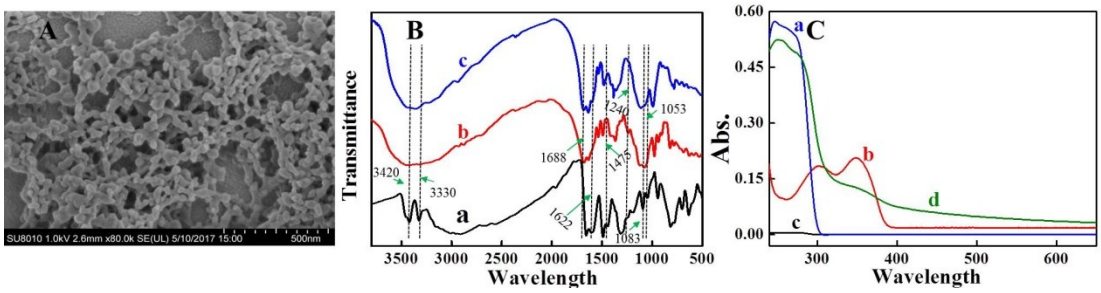

Figure S1. (A) SEM image of theGMP-Tb CPNPs samples. (B) FT-IR spectra of luminol (curve a), GMP (curve b) and luminol-Tb-GMP CPNPs (curve c), respectively. (C) UV–vis spectra of GMP (curve a), luminol (curve b), $Tb(NO_3)_3$ (curve c), and luminol-Tb-GMP CPNPs (curve d), respectively.

The Possible Mechanism of the Dual-Emission Fluorescence Ratiometric Strategy.

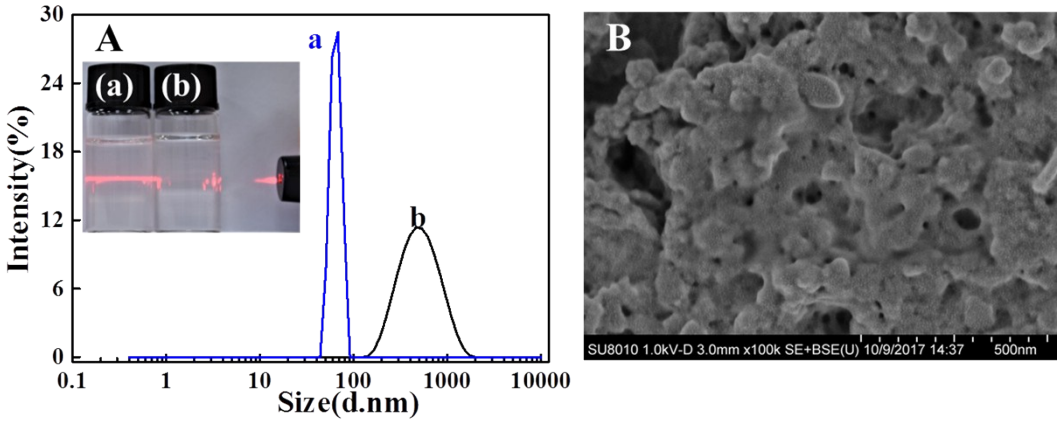

Figure S2. (A) The z-average size of luminol (curve a) and luminol-Tb (curve b). Inset: the Tyndall effect of luminol-Tb (a) and luminol (b), respectively. (B) SEM image of luminol-Tb.

To further ensure the AIE mechanism of luminol with Tb^{3+}, the fluorescence spectra of luminol with different concentrations of Tb^{3+} were examined. The pure luminol emits faint luminescence at 425 nm (Figure S3A). After addition of Tb^{3+} into the luminol solution, the emission of luminol gradually increased with a red-shift of the peak from 425 to 445 nm (blue light emission), owing to the luminol groups formed coordinate-aggregates with Tb^{3+} through metal-to-ligand-charge-transfer.[7] Different from the emission of pure luminol, luminol-Tb exhibits the feature of aggregation-enhanced emission with increasing the concentration of Tb^{3+}, which is a typical feature of AIE mechanism. Furthermore, the fluorescence quantum yield of luminol with different concentration Tb^{3+} was examined. Quinine sulphate is chose as a standard. The optical densities were measured on an UV-2450 spectrophotometer. Absolute values are calculated using the standard reference sample that has a fixed and known fluorescence quantum yield value, according to the following equation:

$$\varphi_X = \varphi_{ST}\left(\frac{M_X}{M_{ST}}\right)\left(\frac{\eta_X}{\eta_{ST}}\right)^2$$

Where the subscripts ST and X denote standard and luminol with Tb^{3+} samples respectively, φ is the quantum yield, M is the gradient of integrated fluorescence vs. absorbance, and η is the refractive indices of the solvents. With increasing the concentration of Tb^{3+} from 0 to 10 mM, the quantum yield of luminol increased gradually as shown in Figure S3B. The highest emission intensity was recorded in its luminol/Tb^{3+} mixtures with the ratio of luminol:Tb^{3+} equal to 1:10 and the fluorescence quantum yields (ϕ_F) value was measured to be 9.64 %, indicating the AIE efficacy of Tb^{3+} to luminol.[8] In addition, the representative fluorescence lifetime decay curves of luminol with different concentrations of Tb^{3+} are further examined as shown in Figure S3C. The lifetime of luminol increases rapidly from 1.487 ns to 12.57 ns upon increasing the Tb3+ concentrations, which is attributed to the coordinating effect induced by Tb^{3+}. As far as we known, in the AIE process, molecular interactions can bring lumophores close together, enabling electronic interactions between the lumophores (e.g. ligand-to-ligand charge transfer), which can cause the spectral shifts, broadening in the emission, loss of vibrionic structure, and increasing emission lifetimes.[7b,8b] This is because of the luminol coordinated with the central metal ions of Tb^{3+}, the linker rigidity of luminol will be increased significantly through metal-to-ligand-charge-transfer. This decreases the non-radiative decay rate and increases the fluorescence intensity of the linker, while allowing spectral shift to be observed.[8b] The decrease in the efficiency of nonradiative pathways is often accompanied with increasing the fluorescence lifetime and quantum yields. Based on those, it can be intuitively understood as the mechanism of this sensor has produced an AIE

phenomenon of luminol by Tb^{3+} in this sensing process.

In order to further confirm the mechanism of this ratiometric fluorescent sensor for ALP detection. Luminol-Tb-GMP CPNPs were then centrifuged and washed with ultrapure water several times to remove free luminol in CPNPs. The depurated luminol-Tb-GMP CPNPs was then incubated by 0.05 U/mL ALP at the same condition as mentioned before. As shown in Figure S3D, compared to the fluorescence spectrum of depurated luminol-Tb-GMP CPNPs (curve a), all peaks of luminol-Tb-GMP CPNPs are decreased with incubated by ALP (curve b), which phenomenon is different of Figure 2. The data presented in Figure S2 is different from the data in Figure 2 because the luminol-Tb-GMP CPNPs in Figure S2 have been centrifuged and depurated to remove free luminol, resulting in different phenomenon of this process as compared to the previous work. The different results of this process indicate that this ratiometric sensor needs to keep luminol excess for occurrence of the AIE phenomenon with the incubation of ALP. This discrepancy further confirms our experimental principle as illustrated in Scheme S1B. After the incubation of ALP, ALP specifically catalyzes the hydrolysis of the phosphate ester group to convert GMP into a guanosine base releasing from CPNPs. Meanwhile, the free luminol in this system re-coordinates with Tb^{3+} after GMP was released. Due to the AIE mechanism of luminol with Tb^{3+}, the fluorescence of luminol increased distinctly and blue light dominated.

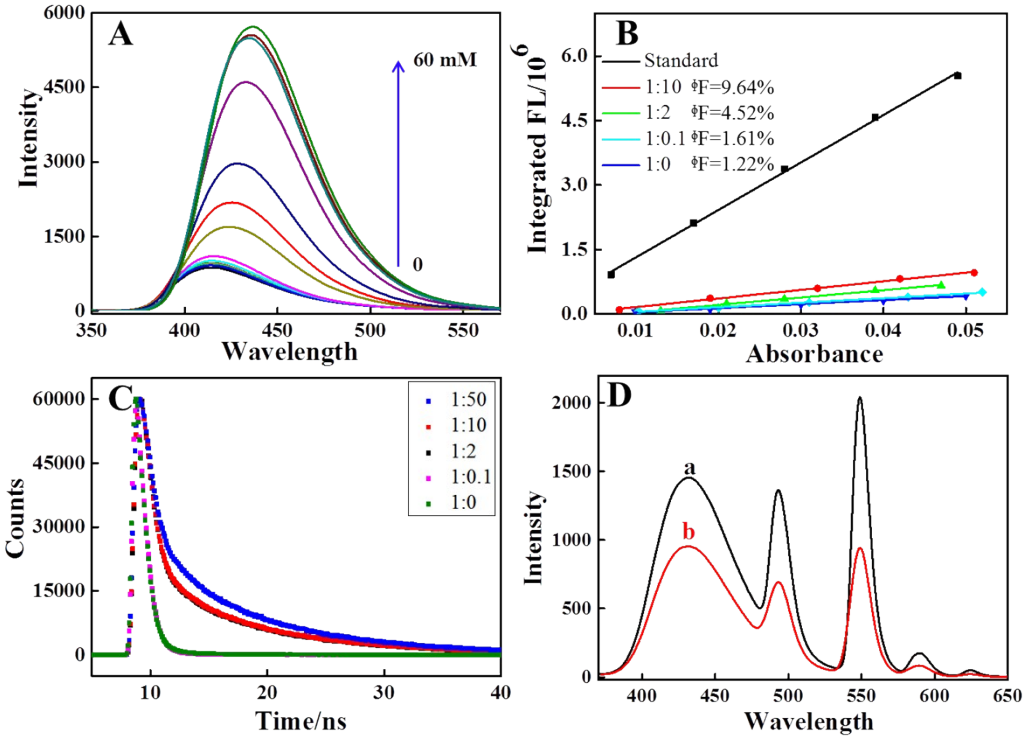

Figure S3. (A) Fluorescence spectra of 0.4 mM luminol with different concentrations Tb^{3+} from 0 to 60 mM. (B) Fluorescence quantum yields (ϕ_F) value of 0.4 mM luminol with different concentrations Tb^{3+} from 0 to 10 mM. (C) Representative fluorescence lifetime decay curves of 0.4 mM luminol with different concentrations Tb^{3+} from 0 to 50 mM. (D) Fluorescence spectra of the depurated luminol-Tb-GMP CPNPs before (curve a) and after (curve b) treated by ALP, respectively.

Optimizing Experimental Conditions. In this work, luminol plays an important role in the sensing process since it is not only enhances the sensitivity of luminol-Tb-GMP CPNPs probe for ALP, but also functions as a response signal. As shown in Figure S4A, with increasing the concentration of luminol, the ratios of F_{549}/F_{432} are decreased (curve a). This is due to luminol coordinate with Tb^{3+} ions that F_{432} of luminol increases and leads to the F_{549} of Tb^{3+} slightly decreased. When addition of 0.05 U/mL ALP into luminol-Tb-GMP CPNPs suspension liquid, the ratios of F_{549}/F_{432} are decreased (curve b). When luminol was controlled at 0.4 mM, the maximum difference valus between

curve a with curve b has gotten. Considering the fluorescence response efficiency and fluorescence intensity of luminol together, the optimal concentration of luminol was chosen at 0.4 mM. The emission spectra of luminol-Tb-GMP CPNPs with pH variation in the absence or presence of ALP were also examined (Figure S4B). In the absence of ALP, the ratio of F_{549}/F_{432} increased with increasing the solution pH (curve a), which is attributed to luminol shows a strong dependence of pH.[9] The maximum emission intensity of luminol fluorescence at low pH values is apparently higher than that at higher pH solutions. In the presence of ALP, F_{549}/F_{432} shows a rapid decrease at pH less than 9, and then increases with further increasing the solution pH (curve b).[9b,9c] We observed that ALP shows a higher performance of this assay at pH of 9 than that of 7.4. Similarly, when pH was chosen at 9, the sensor of luminol-Tb-GMP CPNPs was most sensitive for ALP detection. It indicates that weakly alkaline media is more beneficial for increasing the sensitivity for detecting ALP, because ALP is strongly sensitive to pH. Based on the above analysis, pH of 9 was chosen for further experiments for obtaining high sensitivity for ALP detection.

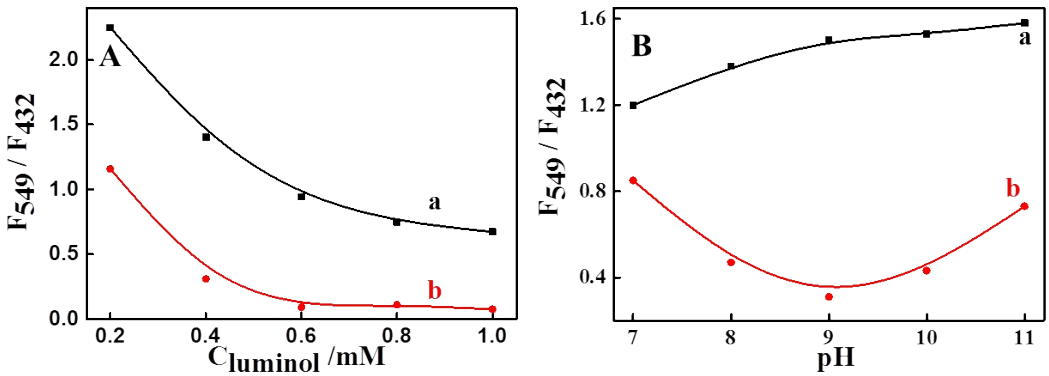

Figure S4. (A) Effects of luminol concentration before (curve a) and after (curve b) on the 0.05 U/mL ALP incubate of luminol-Tb-GMP CPNPs. (B) Effects of different pH before (curve a) and after (curve b) on the 0.05 U/mL ALP incubate of luminol-Tb-

GMP CPNPs. F_{432} and F_{549} are the fluorescence intensities of luminol-Tb-GMP in the wavelength of 432 nm and 549 nm, respectively.

Selectivity and Practical Application for ALP. To evaluate the specificity of the proposed method, the effect of several enzymes was studied, including ALP, thrombin, BSA, IgG, ConA, HRP, Hb, AchE, GA, celluase, Lp. The concentration of ALP was 0.1 U/mL, but all of other enzymes were 10 folds higher than ALP. The ratio of F_{549}/F_{432} shows the maximum change ($F_{549}/F_{432} \approx 0.15$) compared to the blank (luminol-Tb-GMP CPNPs) after addition of the previously listed enzymes that caused by ALP (Figure S5A). These results substantially suggest that these enzymes/proteins do not interfere with the ALP assay with the method developed in this study.

Large amounts of data in literatures indicated that, when dissolved reactive phosphorus (DRP) was in deficiency states, phytoplankton induced the increase of ALP to change organophosphorus into DRP; on the contrary, the high-level DRP inhibited ALP expression rapidly.[10] Therefore, the measurement of ALP is beneficial for detecting DRP level in bodies of water, and ALP could be used as an indicator of the degree of eutrophication in aquatic ecosystems. Having demonstrated the selectivity and sensitivity of our assay for ALP, we next investigated the possibility of applying this assay for dynamic monitoring algal blooms in freshwater lake with ALP as an indicator due to the growth of algal caused by the degree of eutrophication in aquatic ecosystems. As displayed in Figure S5B, the dynamic changes of ALP values of a lake suffering from algal bloom periodically could be easily distinguished by quantified with fluorescence spectra according to the calibration curve obtained before. To ensure the

accuracy of results, the concentration of ALP in water samples was then checked by standard method of alkaline phosphatase kit. The kit was worked by using ALP decomposed sodium benzyl phosphate, which produces free phenol and phosphoric acid. Phenol is oxidized to red quinone derivative by potassium ferricyanide in alkaline solution with 4- amino antipyridine, which can be used to determine the activity of ALP according to the colour and quantify by spectrophotometer. As displayed in Figure S5B inset, the dynamic changes of ALP values of a lake suffering from algal bloom periodically could be easily distinguished by the direct colorimetric visualization with the naked eye from double channels and further quantified with UV−vis spectra. For comparison, the results of these two methods always keep consistent invariably, indicating the reliability of the developed fluorescent method for ALP dynamic monitoring in environmental samples. In Figure S5B, ALP shows a substantial increase (from the 1st to the 9th day); after that, ALP decreases rapidly accompanying with the explosion of algal bloom (from the 9th to the 21th day); finally, it gradually levels off. Through compared with the previous reports, the results obtained with our assay indicate the deterioration of the lake quality is consistent with the actual situation that the whole lake was covered by algal.[11] In addition, compared to the ALP concentration of previous reports on eutrophication of water bodies,[11] indicatting that the degree of eutrophication in Runxi Lake water is not optimistic.

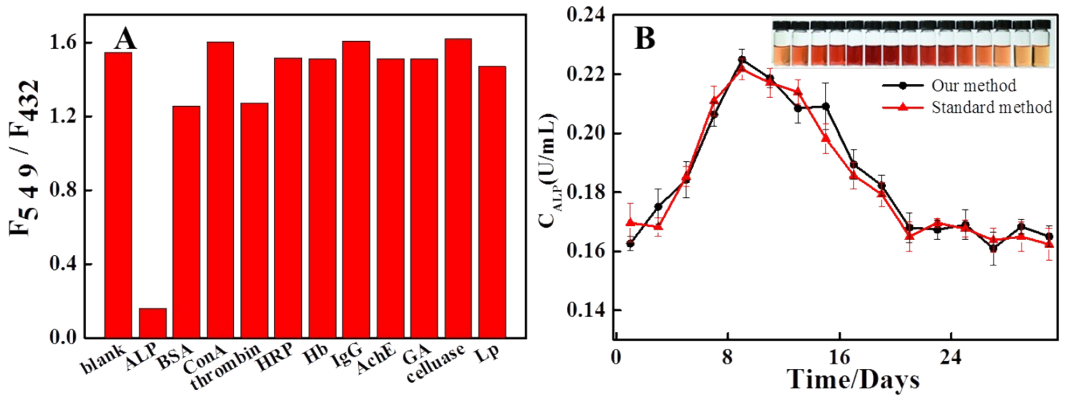

Figure S5. (A) Selectivity of ALP assays in the presence of various analytes. The concentration of ALP was 0.1 U/mL, and was 10 folds lower than other enzymes. (B) Dynamic monitoring of algal blooms in a freshwater lake with APA as indicator. The curve of linear method was calculated by the linear equation. The curve of standard method was obtained by the standard method of colorimetric method. Inset: photograph of the dispersion and supernatant of luminol-Tb-GMP CPNPs with the addition of lake water, from left to right are the days of 1st to 29th, respectively.

Selectivity for Arsenate. To assess the selectivity of luminol-Tb-GMP CPNPs system for arsenate, we examined different metal ions under identical conditions. We used potential interfering analytes (Ba^{2+}, Mn^{2+}, Cd^{2+}, Pb^{2+}, Hg^{2+}, Ag+, As(III), Mg^{2+}, Ca^{2+} NO_3^-, PO_4^{3-}, VO_4^{3-}, dimethoate, DMAA (dimethylarsinic acid), and MMAA (methylarsonic acid)) to investigate the specificity of the arsenate assay. The concentration of arsenate was set at 100 ppb, and the level of other analytes was 10 folds higher than arsenate. The concentration of ALP was final controlled at 0.05 U/mL. As shown in Figure S6, the large intensity change ($F_{549}/F_{432} \approx 1.5$) is caused by arsenate. The interference of other ions is quite tiny, indicating that this ratio fluorescence sensor has high sensitivity and selectivity. But VO_4^{3-}, a conventional

inhibitor for ALP, was usually used in our proof-of-concept experiments, which shows slight disturbances of ALP for As(V) detection.[12] However, the concentration of VO_4^{3-} in real water samples is about 10 ppb, which is 100 times lower in this selective test.[13] And thus, the interference of VO_4^{3-} for As(V) in natural water samples can be ignored. The other organic arsenate of DMAA with MMAA exert tiny effects of the selectivity through the highly inhibition of ALP activity. However, in nature, the organic arsenic is mainly exist in microorganisms and mud, and the dissolved organic arsenic concentrations will not exceed 10% of the total dissolved arsenic on average.[14] In this selective test, the concentration of organic arsenic was up to 1000 ppb, unless the water is heavily contaminated with arsenic, in other cases the interference of organic arsenic can be ignored. The organic pesticides of dimethoate shows slight interference for the detection of As(V). But it is worth noting, except for localized, often accidental, discharges, the quantities of organophosphorus pesticide in the environment are generally about 10 ppt.[15] Such low concentration of organophosphorus pesticide content is very weak to influence As(V) detection in the experiment. These results indicate that the present sensor has higher selectivity for arsenate detection, and this study has broad factual meaning and application prospects.

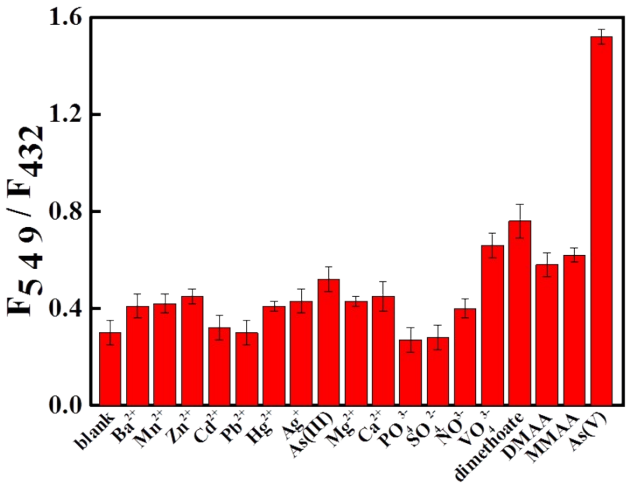

Figure S6. Selectivity of As(V) assay in the presence of various analytes (Ba^{2+}, Mn^{2+}, Zn^{2+}, Cd^{2+}, Pb^{2+}, Hg^{2+}, Ag^{+}, As(III), Mg^{2+}, Ca^{2+} NO_3^-, PO_4^{3-}, VO_4^{3-}, dimethoate, DMAA, MMAA). The concentration of As(V) was 100 ppb, the level of other analytes was 10 folds than As(V). In each analyte, the concentration of ALP was controlled at 0.05 U/mL.

Practical Application for As(V). To test the general applicability of our strategy, spiking recoveries were performed on tap water, Ganjiang River water and Poyang Lake water samples using the standardized method for our assay. With the concentration of ALP controlled at 0.05 U/mL, the concentrations of As(V) in the tested water samples were tested and listed in Table S3. The data show that the analytical recoveries are in an acceptable range of 97.0−105.0%, which is in good agreement with the ICP-MS results with the consistency scope from 96.5−101.9%. The luminol-Tb-GMP CPNPs sensor intra-assay relative standard deviation (RSD) is between 3.9% and 5.1%, which indicates acceptable precision and high accuracy of our fluorescence assay. These results show that this fluorescence assay for the detection of arsenate has potential applications in the analysis of water samples.

Table S1. Various sensing strategies for detection of ALP.

Method	Material	Substrates	LOD (U/mL)	Ref.
Colorimetry	AgNPs	ATP	1	16
Colorimetry	AuNPs	ATP	0.027	17
Electrochemical	Molybdophosphate	ATP	0.0005	18
Electrochemical	Fc	Monophosphate	0.0004	19
Fluorescence	CQDs	ATP	0.0014	20
Fluorescence	Coumarin@Tb-GMP	GMP	0.01	21
Fluorescence	AuNPs@Tb-GMP	GMP	0.0004	11
Fluorescence	Luminol-Tb-GMP CPNPs	GMP	0.00002	This work

Table S2. Various sensing strategies for detection of arsenic.

Method	Materials	Valence	LOD (ppb)	Linear range (ppb)	Ref.
Colorimetry	AuNPs	As(III)	0.5	5-2000	22
Colorimetry	AuNPs/ACP	As(V)	7.5	24.7-75	23
Colorimetry	Citrate-gold NPs	As(III)	1.8	4-100	24
Colorimetry	Molybdate	As(V)	10	-	25
SERS	FeOOH	As(V)	0.0009	0.0075-7500	26
SERS	4-MPY-AgNPs	As(III)	0.76	4-300	27
SERS	Au@Ag NPs	As(III)	0.1	0.5-100	28
Electrochemical	$MnFe_2O_4$	As(III)	1.95	10-100	29
Electrochemical	ACP/polyphenol	As(V)	0.15	5-592	30
Electrochemical	Ascorbic acid	As(V)	0.8	0.94-30	31
Fluorescence	DFPPIC	As(V)	0.075	0.075-7500	32
Fluorescence	APC	As(V)	0.075	0.075-600	33
Fluorescence	Fe_3O_4 NPs	As(V)	3.75	3.75-60	34
Fluorescence	luminol-Tb-GMP CPNPs	As(V)	0.18	0.5-100	This work

- Not mentioned.

Table S3. As(V) detection in different samples by this method and ICP-MS.

Samples	Added	Found (ppb)	Recovery (%)[a]	RSD (n=3, %)	ICP-MS (ppb)	Consistency (%)[b]
Tap water1	0	-	-	-	-	-
Tap water2	1	1.05	105.0	4.8	1.03	101.9
Tap water3	20	19.40	97.0	3.9	20.10	96.5
River water 1	0	-	-	-	-	-
River water 2	1	1.04	104.0	4.3	1.06	98.1
River water 3	20	20.30	101.5	5.1	20.50	99.0
Lake water 1	0	-	-	-	-	-
Lake water 2	1	1.02	102.0	5.0	1.04	98.1
Lake water 3	20	20.01	99.3	4.8	20.40	98.0

[a] Recovery (%) = 100 × (C_{found} /C_{added}). [b] Consistency (%) = 100 × (C_{Found}/C_{ICP-MS}). - Not available.

Reference

1 (a) H. Cui, W. Wang, C. F. Duan, Y. P. Dong, J. Z. Guo, *Chem. – Eur. J.*, 2007, **13**, 6975; (b) H. Duan, L. Li, X. Wang, Y. Wang, J. Li, C. Luo, *New J. Chem.*, 2016, **40**, 458.

2 (a) H. H. Zeng, L. Zhang, L. Q. Rong, R. P. Liang, J. D. Qiu, *Biosens. Bioelectron.*, 2016, **89**, 721; (b) N. Liu, J. Hao, K. Cai, M. Zeng, Z. Huang, L. Chen, B. Peng, P. Li, L. Wang, Y. Song, *Luminescence*, 2018, **33**, 119.

3 H. H. Zeng, W. B. Qiu, L. Zhang, R. P.Liang, J. D. Qiu, *Anal. Chem.*, 2016, **88**, 6342.

4 S. Wang, R. Cazelles, W. C. Liao, M. Vázquez-González, A. Zoabi, R. Abu-Reziq, I. Willner, *Nano Letters*, 2017, **17**, 2043.

5 F. Pu, E. Ju, J. Ren, X. Qu, *Adv. Mater.*, 2014, **26**, 1111.

6 Y. B. Miao, N. Gan, H. X. Ren, T. Li, Y. Cao, F. Hu, Y. Chen, *Talanta*, 2016, **147**, 296.

7 (a) J. Mei, J. Wang, J. Sun, H. Zhao, W. Yuan, C. Deng, S. Chen, B. Z. Tang, *Chem. Sci.*, 2012, **3**, 549; (b) Y. Hong, S. Chen, C. W. T. Leung, J. W. Y. Lam, J. Liu, N. Tseng, R. T. K. Kwok, Y. Yu, Z. Wang, B. Z. Tang, *ACS Appl. Mater. Interfaces* 2011, **3**, 3411.

8 (a) M. Allendorf , C. Bauer, R. Bhaktaa, R. Houka, *Chem. Soc. Rev.*, 2009, **38**, 1330; (b) J. Mei, Y. Hong, J. Lam, A. Qin, Y Tang, B. Tang, *Adv. Mater.*, 2014, **26**, 5429.

9 (a) T. P. Whitehead, G. H. G. Thorpe, T. J. N. Carter, C. Groucutt, L. J. Kricka, *Nature*, 1983, **305**, 158; (b) Y. B. Miao, N. Gan, H. X. Ren, T. Li, Y. Cao, F. Hu, Y. Chen, *Talanta* 2016, **147**, 296 (c) M. Norio, H. Shin-ichi, Y. Kyuichi, M. Hideto, F. Masaru, *Jpn. J. Appl. Phys.* 2001, **40**, 4097

10 (a) A. Vivas, A. Marulanda, M. Go ez, J. M. Barea, R. Azco, *Soil Biol. Biochem.*, 2003, **35**, 987.; (b) C. Labry, D. Delmas, A. Herbland, *J. Exp. Mar. Biol. Ecol.* 2005, **318**, 213.; (c) D. L. Correll, *J. Environ. Qual.,* 1998, **27**, 261.; (d) R. J. ChrO, W. Siuda, G. Z. Halemejko, *Arch Hydrobiol (Suppl)* 1984, **70**, 1.

11 X. Zhang, J. Deng, Y. Xue, G. Shi, T. Zhou, *Environ. Sci. Technol.*, 2016, **50**, 847.
12 F. Zheng, S. Guo, F. Zeng, J. Li, S. Wu, *Anal. Chem.*, 2014, **86**, 9873.
13 Z. Fan, B. Hu, Z. Jiang, *Spectrochimica Acta Part B,* 2005, **60**, 65.
14 W. R. Cullen, K. J. Reimer, *Chem. Rev.*, 1989, **89**, 713.
15 (a) S. Berijani, Y. Assadi, M. Anbia, M. Hosseini, E. Aghaee, *J. Chromatogr. A*, 2006, **1123**, 1; (b) L. He, X. Luo, H. Xie, C. Wang, X. Jiang, K. Lu, *Anal. Chim. Acta*, 2009, **655**, 52.
16 H. Wei, C. Chen, B. Han, E. Wang, *Anal. Chem.*, 2008, **80**, 7051.
17 W. Zhao, W. Chiuman, J. C. Lam, M. A. Brook, Y. Li, *Chem. Commun.*, 2007, **36**, 3729.
18 C. Shen, X. Li, A. Rasooly, L. Guo, K. Zhang, M. Yang, *Biosens. Bioelectron.*, 2016, **85**, 220.
19 S. Goggins, C. Naz, B. J. Marsh, C. G. Frost, *Chem. Commun.*, 2015, **51**, 561.
20 Z. Qian, L. Chai, C. Tang, Y. Huang, J. Chen, H. Feng, *Anal. Chem.*, 2015, **87**, 2966.
21 J. Deng, Y. Ping, Y. Wang, L. Mao, *Anal. Chem.*, 2015, **87**, 3080.
22 R. P. Liang, Z. X. Wang, L. Zhang, J. D. Qiu, *Chemistry – Eur. J.*, 2013, **19**, 5029.
23 J. Zhang, C. Zhang, S. Yu, *ChemPlusChem*, 2016, **81**, 1.
24 L. Gong, B. Du, L. Pan, Q. Liu, K. Yang, W. Wang, H. Zhao, L. Wu, Y. He, *Micro. Acta*, 2017, **184**, 1.
25 J. Das, P. Sarkar, *Environ. Sci.: Water Res.Technol.*, 2016, **2**, 693
26 M. Pradhan, S. Maji, A. K. Sinha, S. Dutta, T. Pal, *J. Mater. Chem. A*, 2015, **3**, 10254
27 J. Li, L. Chen, T. Lou, Y. Wang, *ACS Appl. Mater. Interfaces*, 2011, **3**, 3936.
28 L. Song, K. Mao, X. Zhou, J. Hu, *Talanta*, 2016, **146**, 285.
29 S. F. Zhou, X. J. Han, H. L. Fan, Q. X. Zhang, Y. Q. Liu, *Electrochim. Acta*, 2015, **174**, 1160.
30 S. Cosnier, C. Mousty, X. Cui, X. Yang, S. Dong, *Anal. Chem.*, 2006, **78**, 4985.
31 S. Sanllorente-Méndez, O. Domínguez-Renedo, M. J. Arcos-Martínez, *Talanta*, 2012, **93**, 301.
32 S. Nandi, A. Sahana, B. Sarkar, S. K. Mukhopadhyay, D. Das, *J. Fluoresc.*, 2015, **25**, 1191.
33 A. Banerjee, A. Sahana, S. Lohar, Sukany. Panja, S. K. Mukhopadhyay, D. Das, *RSC Adv.*, 2014, **4**, 3887.
34 B. Liu, J. Liu, *Chem. Commun.*, 2014, **50**, 8568.